DOI: 10.1002/ejic.200500666

A Novel Integrated X-ray Powder Diffraction (XRPD) and Molecular Dynamics (MD) Approach for Modelling Mixed-Metal (Zn, Al) Layered Double Hydroxides (LDHs)

Giuseppe M. Lombardo,[a] Giuseppe C. Pappalardo,*[a] Francesco Punzo,[a] Ferdinando Costantino,[b] Umberto Costantino,[b] and Michele Sisani[b]

Keywords: Layered double hydroxides / Molecular dynamics / X-ray diffraction / Structure elucidation

A combination of experimental (XRPD) and computational (MD-simulation) techniques was used for a detailed study of the structural, dynamic and hydration properties of the ZnAl layered double hydroxides (LDHs) of formula $[Zn_{0.65}Al_{0.35}(OH)_2]Cl_{0.35}\cdot yH_2O$ (**I**) and $[Zn_{0.65}Al_{0.35}(OH)_2](CO_3)_{0.175}\cdot yH_2O$ (**II**), with y = 0.35 and 0.69, respectively. Our approach was based on a direct comparison made, for the first time, between the observed XRPD diffraction pattern and the MD-simulated pattern of each model that was considered. The XRPD curve is affected (reflection angles and line shapes) by dynamic and structural factors, and the interlayer distribution of the water content. Accordingly, its reproduction through MD modelling is the most suitable means of monitoring these properties of the material. Molecular modelling was performed by MD simulations of models of **I** and **II** built up through appropriate modifications of their interlayer total water contents and related distribution. The validated models, namely those that provided the best MD-simulated pattern of **I** and **II**, were then used to determine structures and features which have not been previously determined by conventional diffraction techniques. The calculated XRPD curves were corrected to take into account the "size" broadening effect. The approach provided structural data that matched well those obtained by Rietveld analyses for the usual parameters. Furthermore, the study was original in its capability to detect and thus to discriminate between the different interatomic distances Zn–O, Al–O, Al···Al, Zn···Zn, Zn···Al in the slabs. The MD-simulated models of **I** and **II** provided the best reproduction of the XRPD curves for total water of hydration contents of y = 0.25 and y = 0.69, respectively. In the case of **II**, a domain with a homogeneous distribution of total water contents predominated. Conversely, in the case of **I**, a nonhomogeneous distribution featured by two (or multiple) shared crystalline domains having different interlayer water contents was evidenced.

Introduction

Layered double hydroxides (LDHs), also known as anionic clays or hydrotalcite-like compounds (HTlc), are solid compounds having positively charged layers and intercalated exchangeable interlayer anions to maintain charge neutrality.[1–11] Their general formula is $[M^{II}_{1-x}M^{III}_{x}(OH)_2]^{x+}(A^{n-}_{x/n})^{x-}\cdot yH_2O$ in which M^{II} = Mg, Zn, Co, Ni, Mn, etc., M^{III} = Cr, Fe, V, Co, etc., A^{n-} = an inorganic or organic anion of charge *n*.

The great technological relevance of LDHs stems from their use as precursors in catalysis.[7,10,12–16] In particular, ternary LDHs of type $[Cu_yZn_{1-x-y}Al_x(OH)_2](CO_3)_{x/2}\cdot(1-3x/2)H_2O$, after thermal decomposition and successive reduction of the copper oxide to the metal with hydrogen, attain a tight mixture of oxides with copper particles ($Cu/ZnO/Al_2O_3$) that is active as a catalyst for hydrogen production from oxidative steam reforming of methanol (OSRM). This is useful for developing a clean power source for vehicles.[17–19]

Understanding the structural and dynamic properties of this important class of materials is a central issue in studies focusing on the design of second-generation LDH precursors and derived catalysts with enhanced or new performances.

The arrangement of the interlayer species is not well understood and is difficult to probe experimentally. It frequently happens that anions and water molecules associate strongly with particle surfaces, and some adsorbed water molecules are indistinguishable from interlayer water in thermal analyses.

---

[a] Dipartimento di Scienze Chimiche, Facoltà di Farmacia, Cattedra di Chimica Generale ed Inorganica, Università di Catania, Viale A. Doria 8, 95125 Catania, Italy
E-mail: gcpappalardo@dipchi.unict.it
[b] CEMIN Centro di Eccellenza Materiali Innovativi Nanostrutturati, Dipartimento di Chimica, Università di Perugia, Via Elce di Sotto 8, 06123 Perugia, Italy

Unfortunately, these materials are obtained only as powders, often with a low degree of crystallinity, thus making structural determinations by single-crystal X-ray analysis impossible. Further, even in cases where the powdered solids initially exhibit a high degree of crystallinity, large overlapping bands from relatively poor diffraction patterns are often observed when these solids are modified by heating, ion-exchange, intercalation, pillaring or topotactic functionalisation by ligand substitution. Therefore, detailed structural information on these systems from X-ray powder diffraction (XRPD) data is difficult to obtain or otherwise inaccessible.

We have recently used molecular dynamics (MD), combined with large angle X-ray scattering (LAXS)[20–24] or XRPD experiments,[25,26] for determining structural parameters (molecular assembly, interatomic and intermolecular distances).

Application of MD for simulating these materials provides the following: (i) an ability to monitor the internal molecular fluctuations, thus revealing, by implementing high-temperature MD runs, processes leading to metal segregation and to the breakdown of the structure of the precursor; (ii) the ability to generate microscopic-level structural information that can be correlated directly with the experimentally detectable activity and selectivity of catalysts for OSRM; (iii) the capacity to refine molecular structures by using experimental data, especially from X-ray diffraction experiments for microcrystalline and amorphous solid phases.

The ability to predict macroscopic properties of HTlc on the basis of microscopic structures derived from MD simulations has a fundamental impact on the design of new materials with improved technological requisites. To accomplish this, not only should the molecular simulations be carried out on a long enough time scale to sample a significant volume of phase space, but also: (i) a suitable unit or fragment of the material should be selected to serve as the model of the real system; and (ii) the force field (FF) used by the MD program should feature a high-quality parameterisation developed ad hoc for the system that is being dealt with.

Previous computer modelling focused on interlayer distance dynamics in binary LDH systems[27–32] by using generic force fields. Quite recently, a force field (CLAYFF) designed for simulations of clay phases was optimised on the basis of known mineral structures for the Si, Al, Mg, Ca, Fe and Li species.[33] In order to model binary Zn-containing LDHs by using MD simulations for the first time, we relied on a modified version of the CLAYFF into which suitable ad hoc developed Zn parameters were inserted.

The models used for the simulations (Figure 1) of $[Zn_{0.65}Al_{0.35}(OH)_2]Cl_{0.35}\cdot 0.35H_2O$ (**I**) and $[Zn_{0.65}Al_{0.35}(OH)_2](CO_3)_{0.175}\cdot 0.69H_2O$ (**II**) were preliminarily validated on the basis of a direct agreement between the experimental XRPD patterns and those calculated from MD. The calculated XRPD patterns were obtained by averaging patterns calculated from snapshots collected along the entire evolution time of the MD simulation for each of the models considered. By this procedure, the positions of the observed diffraction lines could be reproduced by taking the thermal, dynamic and structural factors, as well as the water content of the material into account.

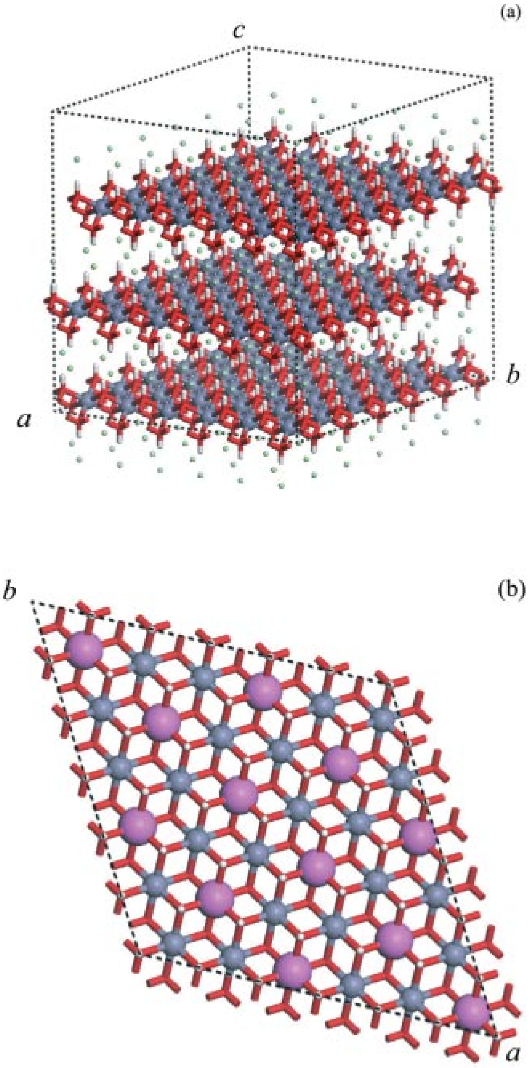

Figure 1. (a) The 3-layered model supercell with independent variables *a*, *b*, *c*, *α*, *β*, *γ* used for the MD simulations of both the LDHs **I** and **II**. The green balls represent the positions available for accommodation of interlayer water molecules with chloride (**I**) or carbonate (**II**) anions. (b) View of the preferred planar arrangement of metallic ions in the Zn/Al slab in the ratio 2:1 (element colours: Zn blue-grey; Al pink; O red, H white).

In the present study the combined approach, validated as stated above, was used for featuring the LDHs **I** and **II** in terms of structure, dynamics and arrangement of their interlayer water molecules and anionic species.

Results and Discussion

Analysis of XRPD Patterns

The Rietveld plots and crystallographic data obtained from the XRPD patterns of the well-crystallised samples of **I** and **II** are given in Figure 2 and Table 1, respectively.

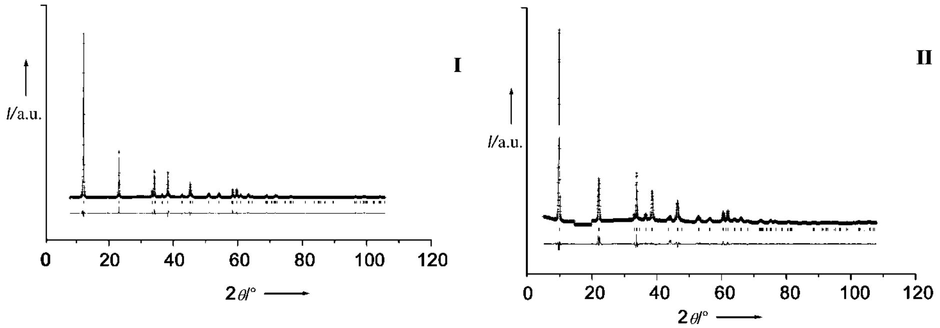

Figure 2. Rietveld plots for **I** and **II**; experimental (+), calculated (–) and difference (lower) profiles.

Table 2 contains the atomic parameters and main geometrical data of compounds **I** and **II**. These results show a good general agreement with those already known in the literature for analogous HTlc.[9,10] The relative positions of the atoms inside the unit cells, as attained by the fractional coordinates given in Table 1 and Table 2, and their relative images due to the *R*3*m* symmetry are depicted in Figure 3.

Table 1. Crystallographic data for $[Zn_{0.65}Al_{0.35}(OH)_2](Cl)_{0.35}\cdot0.35H_2O$ (**I**) and $[Zn_{0.65}Al_{0.35}(OH)_2](CO_3)_{0.175}\cdot0.69H_2O$ (**II**) from Rietveld analysis.

	I	II
Space group	*R*3*m*	*R*3*m*
a [Å]	3.07497(6)	3.0758(1)
c [Å]	23.1524(5)	22.8089(8)
Cell volume [Å^3]	189.588(6)	186.87(1)
Z	3	3
Calculated density [g cm^{-3}]	2.759	2.904
Unit cell formula weight	315.0	326.7
R_{wp}[a]	0.119	0.104
R_p[b]	0.088	0.071
R_F[c]	0.076	0.086
χ[d]	4.7	7.9

[a] $R_p = \Sigma|I_o - I_c| / \Sigma I_o$. [b] $R_{wp} = \{\Sigma[w(I_o - I_c)^2] / \Sigma[wI_o^2]\}^{1/2}$. [c] $R_{F^2} = \Sigma|F_o^2 - F_c^2| / \Sigma|F_o^2|$. [d] $\chi = \{\Sigma[w(I_o - I_c)^2] / (N_o - N_{var})\}^{1/2}$.

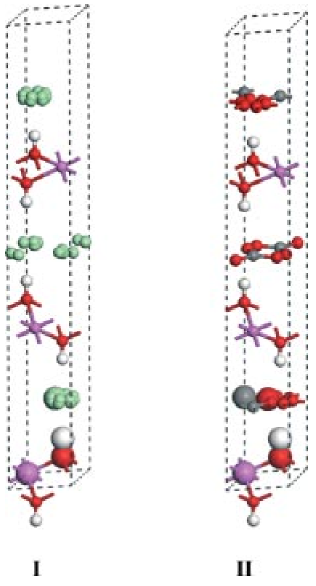

Figure 3. Spatial distributions of atoms in the cells of **I** and **II** obtained from Rietveld analyses. The atoms whose positional parameters were achieved using the Rietveld analyses are evidenced by larger spheres; the atomic positions generated by *R*3*m* symmetry are denoted by smaller spheres. Zn, Al pink; O, red; Cl, green; C, grey; H, white.

Table 2. Positional and thermal parameters for **I** and **II**.

Atom	*x*/*a*	*y*/*b*	*z*/*c*	100U_{iso} [Å^2][a]	Wyckoff notation	Occupancy	Number of atoms per cell
			I $[Zn_{0.65}Al_{0.35}(OH)_2](Cl)_{0.35}\cdot0.35H_2O$				
Zn	0.0	0.0	0.0	2.21(4)	3a	0.65	2
Al	0.0	0.0	0.0	2.21(4)	3a	0.35	1
O(1)	0.0	0.0	0.3745(1)	3.3(1)	6c	1	6
O(2)	0.1586(12)	–0.3172(23)	0.1676(7)	8.8(5)	18h	0.056	1
Cl	0.1586(12)	–0.3172(23)	0.1676(7)	8.8(5)	18h	0.056	1
H	0.0	0.0	0.4135(5)	3.3(1)	6c	1	6
			II $[Zn_{0.65}Al_{0.35}(OH)_2](CO_3)_{0.175}\cdot0.69H_2O$				
Zn	0.0	0.0	0.0	2.15(9)	3a	0.65	2
Al	0.0	0.0	0.0	2.15(9)	3a	0.35	1
O(1)	0.0	0.0	0.3740(2)	3.4(2)	6c	1	6
O(2)	0.1137(15)	–0.1137(15)	0.5004(14)	3.4(2)	18h	1/6	3
C	1/3	2/3	0.5004(14)	3.4(2)	6c	1/12	0.5
H	0.0	0.0	0.4142(6)	3.4(2)	6c	1	6

[a] U_{iso} = mean square displacement, $B_{iso} = 8\pi^2\ U_{iso}$.

In both samples the hydroxy groups are coordinated to the metal (octahedral) pointing alternatively upwards and downwards from the layer, giving rise to three cavities in the interlayer region around each metal on both sides of the layer. The chloride anions occupy a single site in the unit cell of **I**, whereas the carbonate anions are arranged parallel to the layer and occupy three sites with the oxygen atoms in the unit cell of **II**. This determines, assuming that ionic exchange is the same, a greater number of positions available for the water of hydration in the chloride phase.

MD Simulations of XRPD Patterns

The examination of the whole series of simulations was performed in terms of comparisons between the calculated and experimental XRPD patterns. The best MD simulations of the XRPD patterns of compounds **I** and **II** were achieved for models containing 27 (y = 0.25) and 75 (y = 0.69) water molecules, respectively. Measures of similarity (R_{wp}) between experimental and MD-simulated patterns as a function of the total water contents y are quoted in Figure 4. All the experimental peak positions were located well by MD, whereas, as expected, the peak heights and line shapes did not exactly reproduce the experimental curves of either **I** or **II**. The heights of the calculated peaks are lower than the experimental ones. This is typical in the case of the occurrence of very thin microcrystals (exfoliation along the c axis) for which: (i) the intensity of the first peak (003) decreases significantly, and (ii) the normalisation with respect to this small angle peak determines the higher intensities at the large angle portion of the pattern. Further, the MD simulations of the crystal (see forthcoming section Structural Data) reveal the skidding of the c planes and the important concerted fluctuations, which affects the entire set of cell parameters. A further contribution to such a discrepancy comes from the restricted spanning of the phase space resulting from the small size of the simulated models. In fact, the interlayer species of the models cannot attain all the reticular positions made available by the Rietveld analysis in the $R3m$ symmetry (Figure 3). Figure 5 shows the XRPD patterns of **I** and **II** compared with the simulated ones after corrections have been made for crystallite size broadening (see Computational Details).

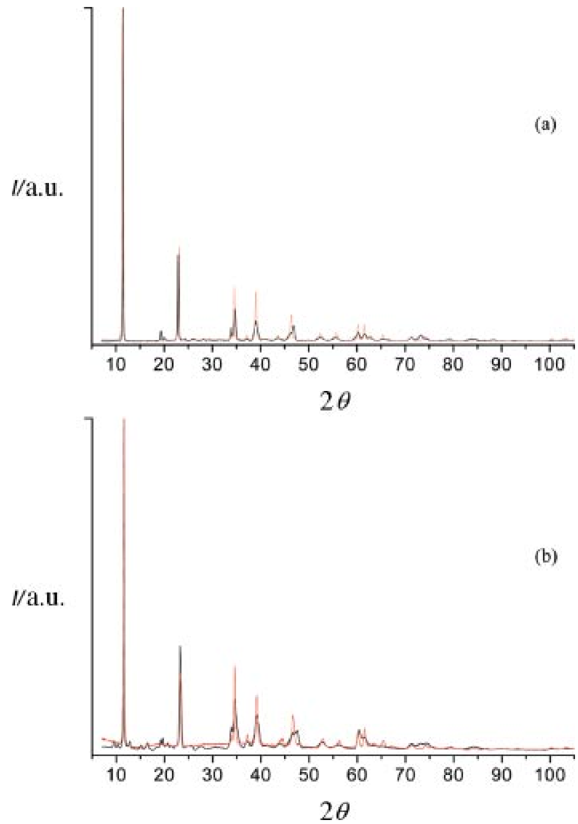

Figure 5. Comparison of experimental (red) and MD-simulated (black) XRPD patterns of **I** (a) and **II** (b).

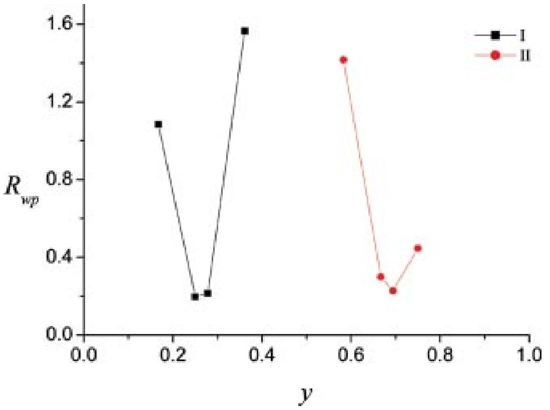

Figure 4. A measure of the similarity (R_{wp}) between experimental and MD-simulated patterns as a function of the total water content y. The minima show that the models which best reproduce the XRPD patterns of **I** and **II** have formula coefficients y = 0.25 and y = 0.69, respectively.

Hydration Properties

The MD runs showed that the simulated models of **I** and **II** having total water of hydration contents of 27 (y = 0.25) and 75 (y = 0.69), respectively, were the best at reproducing the experimental XRPD curves. In the case of the carbonate compound **II**, the MD simulation attained a value of the averaged empirical formula coefficient y = 0.69 for reproducing the experimental data of the sample as determined by using TG analysis. This corresponds to the model in which the water molecules (N_w = 75) are distributed in a homogeneous fashion, i.e. as three sets of 25 water molecules per interlayer.

In the case of the chloride compound **I** the theoretical model having a total N_w of 27 (y = 0.25) distributed as nine

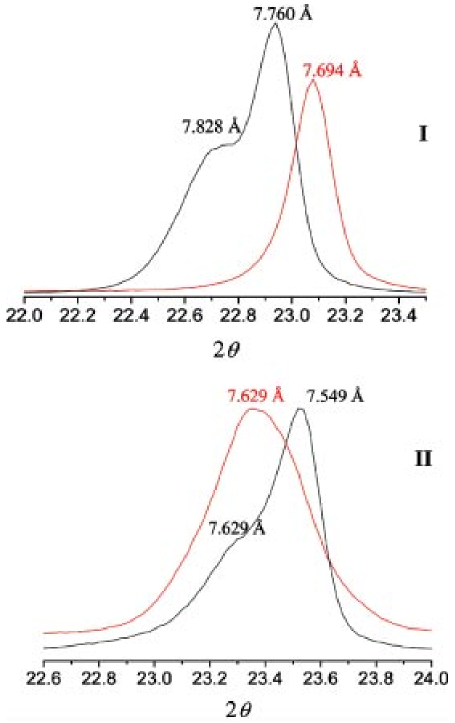

Figure 6. Detailed view of the (006) peaks of the treated (red) and nontreated (black) samples of **I** and **II**. The interlayer distances [Å] are indicated on the corresponding peaks and shoulders of the curves. This multiplicity collapsed into a well-resolved single peak shifted to a higher ($2\theta = 23.1°$) and lower angle ($2\theta = 23.3°$) in the case of the treated samples **I** and **II**, respectively. In **I** the treated sample gave rise to a single peak due to water loss; in **II** the treated sample took on a single peak shape due to the decreased size of the microcrystals and a shift towards increasing water content in the interlayer. In fact, the raised baseline and the broader peak denote the formation of amorphous material due to disaggregation resulting from the exfoliation process of the layers after the treatment.

water molecules per interlayer does not coincide with the average formula index value $y = 0.35$ measured for the synthesized sample. By keeping in mind that all the simulated models featured a regular interlayer distribution of the total number of water molecules, N_w, and that the MD simulation of the model $N_w = 27$ corresponds well with the experimental pattern, the observed discrepancy in the water contents between the experimental formula index value measured by TGA ($y = 0.35$) and the theoretical value ($y = 0.25$) can be accounted for in terms of a predominantly heterogeneous distribution of the water content in the interlayer of the material. Further evidence for this was provided by the (006) peaks observed in the XRPD patterns at ca. $2\theta = 23.0°$ of the freshly prepared samples of **I** and **II**, both showing a marked shoulder (Figure 6). This multiplicity is consistent with two (or multiple) shared crystalline domains that have different water contents in the interlayer. The above findings are consistent with the results provided by the averaged total energies calculated from MD trajectories of the models of **I** and **II** at the various arrangements (Table 3; Figure 7). These results confirmed on an energy basis that: (i) the approach is sensitive to the more or less homogeneous distribution of the total water content in the interlayer; (ii) in the case of **I** the most heterogeneous interlayer water arrangement is the predominant motif; (iii) in the case of **II** the homogeneous motif predominates at the values of total water content measured by thermogravimetric techniques ($y = 0.69$); and (iv) in the case of both **I** and **II**, for total water contents higher than the measured ones, a more heterogeneous interlayer distribution of the water contents is predicted on the basis of the force field that was used. The theoretical relationship between interlayer distance and total water content is shown in Figure 8.

Table 3. MD-calculated total average energies (E, kcal mol^{-1}) assuming different interlayer distributions of the water molecules (N_w) for models of **I** and **II**.

I				**II**			
$[Zn_{0.65}Al_{0.35}(OH)_2](Cl)_{0.35}\cdot{<}y{>}H_2O$				$[Zn_{0.65}Al_{0.35}(OH)_2](CO_3)_{0.175}\cdot{<}y{>}H_2O$			
$<y> = 0.361$				$<y> = 0.694$			
Layer	N_w	y	E	Layer	N_w	y	E
1	13	0.361		1	25	0.694	
2	13	0.361	–31943.086	2	25	0.694	–35522.575
3	13	0.361		3	25	0.694	
1	10	0.278		1	22	0.611	
2	19	0.528	–31945.351	2	31	0.861	–35520.586
3	10	0.278		3	22	0.611	
1	7	0.194		1	19	0.528	
2	25	0.694	–31970.793	2	37	1.028	–35517.807
3	7	0.194		3	19	0.528	
$<y> = 0.500$				$<y> = 0.861$			
Layer	N_w	y	E	Layer	N_w	y	E
1	18	0.500		1	31	0.861	
2	18	0.500	–32058.498	2	31	0.861	–35574.264
3	18	0.500		3	31	0.861	
1	15	0.417		1	28	0.777	
2	24	0.666	–32077.331	2	37	1.028	–35584.367
3	15	0.417		3	28	0.777	
1	12	0.333		1	25	0.694	
2	30	0.833	–32076.940	2	43	1.194	–35646.050
3	12	0.333		3	25	0.694	

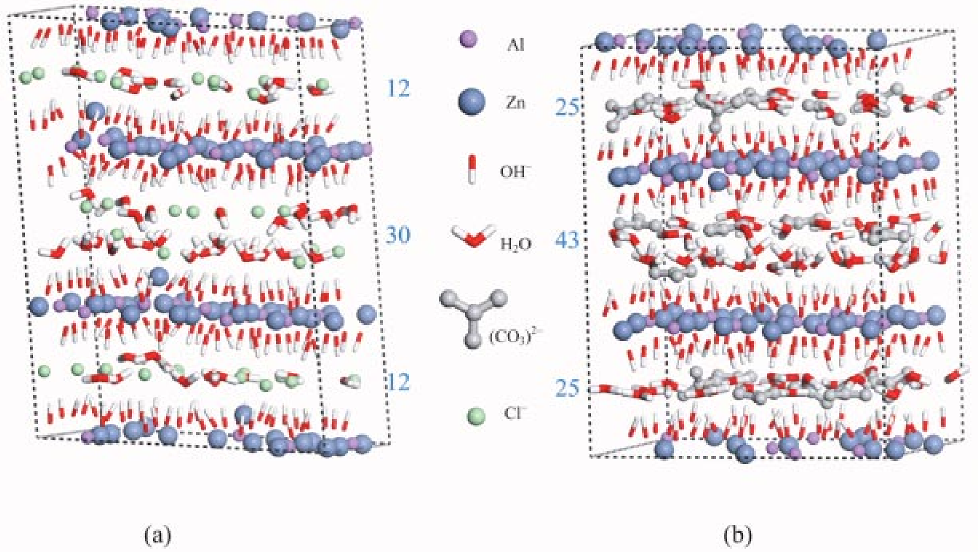

Figure 7. Example of models of **I** (a) and **II** (b) with y = 0.500 and y = 0.861, respectively (snapshot after the 200-ps simulation). The nonhomogeneous distribution of water molecules between the layers (see Table 3) is shown here by the blue numbers along the *c* axis. The notation used for atoms and interlayer species (water and anions) is given in colours.

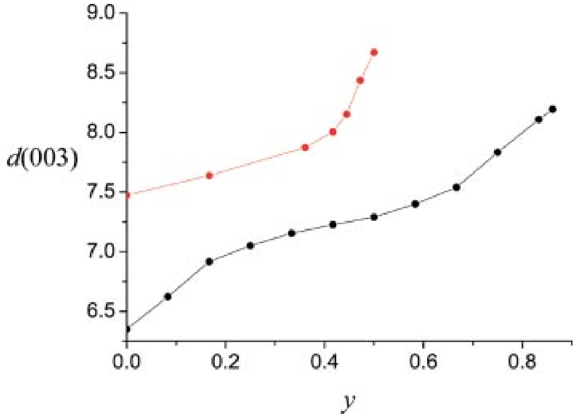

Figure 8. MD-calculated (averaged collection of 200-ps trajectories) interlayer distances [*d*(003)] in **I** (red) and **II** (black) as a function of the total interlayer water content.

Structural Data

The acceptable agreement of the interatomic distances calculated from MD with those provided by Rietveld analyses is shown in Table 4. This constitutes a further validation of the good quality of the FF used and consequently of the whole combined approach. The MD analyses of both **I** and **II** provide a complete set of layer interatomic distances (Zn–O, Zn···Zn, Zn···Al) that agree with those available from EXAFS experiments on the nitrate analogues (Table 4). Furthermore, the analysis of the trajectories of the models of **I** and **II** bearing y = 0.25 and y = 0.69 water molecules, respectively, which produced the best MD reproduction of the experimental XRPD pattern, provided (Figure 9a and b) microscopic information concerning: (i) the fluctuating orientation (from parallel to perpendicular) of the interlayer planar moieties of the CO_3^{2-} anions, (ii) the effective ten-

Table 4. MD-calculated average interatomic distances [Å] compared with those obtained from Rietveld analyses for models of **I** and **II**. EXAFS[41] data available for the analogous LDHs $(Zn_xAl_{1-x})(OH)_2(NO_3)\cdot(1-x)H_2O$ are quoted for the purpose of comparison.

	MD		Rietveld		EXAFS[41]
	I	**II**	**I**	**II**	
Zn–O(1)	2.080	2.059	2.015	2.003	2.07
Al–O(1)	1.970	1.963	2.015	2.003	
Zn–Zn	3.078	3.090	3.074	3.076	3.10
	5.321	5.335	5.328	5.327	
Al–Al	5.316	5.317	5.326	5.327	
Zn–Al	3.067	3.075	3.076	3.076	3.06
O(1)–Cl,C	3.207	3.148	3.030	3.386	
O(2)–Cl,C	3.191	3.161			
O(1)–O(1)	2.750	2.756	2.622	2.568	
O(1)–O(2)	2.785	2.766	2.879	2.937	
Zn–Cl,C	2.196	2.225			
	4.060	4.179	4.004	3.790/4.204	
Al–Cl,C	4.792	4.215	4.004	3.790/4.204	
		4.927			
Cl–Cl, C–C	4.312	4.179			

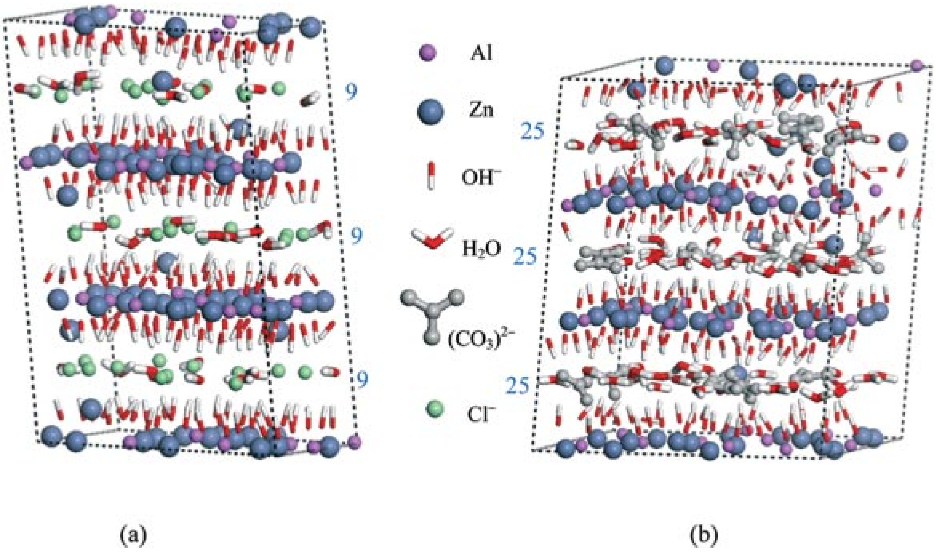

Figure 9. Perspective view of the supercells of **I** (a) and **II** (b) with $y = 0.25$ and $y = 0.69$, respectively, (snapshot after the 1-ns simulation) which best reproduce the experimental patterns. The homogeneous distribution of water molecules between the layers is indicated here by the blue numbers along the *c* axis. The notation used for the atoms and interlayer species (water and anions) is given in colours.

dency of the Zn atoms to segregate in the samples of both compounds **I** and **II**, (iii) the interlayer H_2O molecules of **I** and **II** that fluctuate about the coplanar arrangement with respect to the layer; and (iv) the dynamics of the layer as determined by the concerted sliding of the slabs about the equilibrium position.

Conclusions

The structural features, dynamics and arrangement of the interlayer species (total water content and anions) for the ZnAl hydrotalcite-like compounds in the chloride (**I**) and carbonate (**II**) forms were studied by using experimental (XRPD, TGA) and computational (MD) techniques in a complementary fashion. To this purpose we first implemented, for the systems in which Me(II) = Zn, a set of parameters from the recent CLAYFF force field[34] that included suitable parameters for LDH species. The structural data coming from the XRPD Rietveld analyses were in agreement with the MD results, thus providing a first validation of the FF parameters that were used.

The main findings of the present work revealed: (i) the general ability of this approach to monitor microscopic-level properties such as the guest orientations, their fluctuations and the interlayer arrangement in the studied LDHs; (ii) the ability to detect and thus to discriminate between the different interatomic distances (Zn–O, Al–O, Al···Al, Zn···Zn, Zn···Al) of the slab, in a manner independent from other X-ray diffraction techniques such as EXAFS; (iii) the tendency of the zinc atoms to segregate, which occurs in both compounds **I** and **II**; (iv) the tendency of compound **I** to adopt a heterogeneous interlayer distribution of water. This heterogeneous distribution, although it includes domains having $y = 0.25$, leads to a higher average formula index value (y) in compound **I**; (v) that the crystal size of **I** remained unaffected by dehydration (even down to $y = 0$) of the material; (vi) that material **II** preferred the homogeneous distribution (25 per interlayer) of the experimental total water content ($y = 0.69$); (vii) the fact that, for the same reason as in (iv), the crystal was likely to disaggregate through exfoliation of the *c* layers, leading to water loss and consequently a smaller size of the microcrystals; and (viii) the capability of the computational approach to indicate with good accuracy the interlayer water distribution of the material.

In conclusion, the following general issues were achieved: first, a nonexpensive approach, which shows the tendency of LDHs to attain structures bearing heterogeneous or homogeneous interlayer distribution of their total water contents, and second, the symbiosis between experiment and theory that played a role in validating MD-simulated structure models of LDHs through direct matching of the experimental XRPD patterns. The direct reproduction of the diffraction pattern made possible a model that accounts for microscopic thermal, dynamic and structural factors, in addition to water-content distribution of the material being studied.

Experimental Section

Preparation of the Samples: A large batch of Zn–Al hydrotalcite-like compound, with the formula $[Zn_{0.65}Al_{0.35}(OH)_2]$-$(CO_3)_{0.175}\cdot 0.69H_2O$ (**II**), was prepared by the urea method[9] according to the following procedure: a clear solution, obtained by mixing $AlCl_3$ (100 mL, 0.50 M), $ZnCl_2$ (200 mL, 0.50 M) and urea (30 g), was maintained at reflux temperature for 3 d. The precipitate obtained was filtered, washed with deionised water and equilibrated, whilst stirring, with Na_2CO_3 (100 mL, 0.1 M) for 1 d in order to exchange the chloride ions (sometimes incorporated during the synthetic procedure) with carbonate ions. After equilibration, the solid was recovered, washed with deionised water, and finally dried and stored over P_4O_{10} in the presence of soda lime.

The Zn–Al hydrotalcite-like compound in the chloride form, $[Zn_{0.65}Al_{0.35}(OH)_2]Cl_{0.35}\cdot 0.35H_2O$ (**I**), was obtained by titrating the carbonate form, previously dispersed in NaCl (0.1 M, mass/volume ratio 1 g 50 mL^{-1}), with HCl (0.1 M) by means of a Radiometer automatic titrator operating in the pH stat mode and at pH 5. The solid was washed with CO_2-free deionized water and stored over P_4O_{10} in the presence of soda lime.

Analytical Procedures: The metal ion content of HTlc was determined by ion chromatography, after dissolution of about 100 mg of sample in concentrated HCl. The metal ion concentration in the resulting solution was measured by the following procedures: (i) Zn content: column Dionex CS5a, eluent PDCA, flow 1.0 mL min^{-1}, spectrophotometric detection after Post Column Reaction (PCR) with PAR; (ii) Al content: column Dionex CS5a, eluent HCl (0.75 M), flow 1 mL min^{-1}, spectrophotometric detection after PCR with Tiron. The chloride content was determined by ion chromatography for the solution obtained by soaking the solid samples in Na_2CO_3 (1 M) at 80 °C for 4 h. C and H elemental analysis was performed with a Carlo Erba 1106 analyser. Carbonate and water contents were also evaluated from TGA.

Characterisation: X-ray powder patterns were collected in the 7–110° and 0.02° step size (2θ range) according to the step scanning procedure using Cu-K_α radiation with a Philips X'Pert APD diffractometer, PW3020 goniometer equipped with a bent graphite monochromator on the diffracted beam. Divergence and scatter slits of 0.5° and a receiving slit of 0.1 mm were used. The LFF ceramic tube operated at 40 kV and 30 mA. To minimise preferred orientations, the sample was carefully side loaded onto an aluminium sample holder with an oriented quartz monocrystal underneath. The counting time was 20 sec step^{-1} for all the diffraction patterns. The TG/DTG/DTA analyses were performed in air with a Netzsch STA449C thermal analyser at a heating rate of 5 °C min^{-1} under an air flow.

Rietveld Refinement: Rietveld refinements for **I** and **II** were performed using the GSAS program.[34] Sample displacement, cell parameters and background were first refined. Fractional coordinates and isotropic thermal factors for all the atoms, and profile shape were also refined. The profile was modelled using a pseudo Voigt profile function (six terms) with two terms for the modelling of asymmetry at low 2θ angle. The interatomic distances and bond lengths were refined freely, except for the O–H distance that was restrained to 0.9(3) Å. Isotropic thermal factors were refined by constraining the program to apply the same shift to the metal atoms and another shift to the light atoms. The metal atom occupancies were set at fixed values (according to the stoichiometry) and were not refined. At the end of the refinement the shifts on all parameters were less than their standard deviations.

Computational Details

FF Parameters: The Materials Studio package (Accelrys Inc., San Diego) was used to perform all MD simulations through the Discover module. In the present work, the recently developed CLAYFF force field[34] was included. This FF features suitable parameters for LDHs containing the Si, Al, Mg, Ca, Fe and Li species. Accordingly, to overcome the lack of parameters for systems in which Me(II) = Zn, the Zn parameters were derived by using the following minerals, for which structural data are available, as model compounds: ε-$Zn(OH)_2$[35,36] γ-$Zn(OH)_2$,[37] $Zn_5(OH)_8Cl_2\cdot H_2O$.[38] For the VDW function, the following parameters were obtained: $D_0 = 1.0\times10^{-6}$ kcal mol^{-1}, $R_0 = 5.0$ Å, charge = 1.05 *e*. The orders of magnitude of these calculated Zn nonbonding parameters were in agreement with those of the species Si, Al, Mg, Ca, Fe, Li as quoted in Table 1 of ref.[34]. The parameter values of the electrostatic terms reported in this table were readjusted as follows: hydroxy oxygen (OH) = –0.875 *e*; aqueous chloride ion (Cl^-) = –0.975 *e*, on the basis of the hydrotalcite-type structure used for modelling. This was done in order to achieve total electroneutrality through the redistribution of the charge on Al among the surrounding hydroxy groups.

Protocols: The MD simulations started from the energy-minimised structures. The periodic boundary conditions (PBC) with an NPT ensemble were used for all the runs. Transients of 200 ps and 1 ns were collected for the models at various hydration degrees and for the models selected for the validation procedure of the simulations, respectively. In both cases the integration time step was 0.001 ps, and the sampling interval was 1000 time steps. The energy-optimised structures were obtained with the smart minimiser of the Discover module, satisfying a gradient of 0.1 kJ mol^{-1}. The nonbonding (NB) settings were those provided by default in this module for VDW interaction: atom-based summation method with cutoff = 9.5 Å, spline width = 1.0, buffer width = 0.50, and long-range energy correction = 9.5. For the Coulomb interaction, an Ewald summation method was used with accuracy = 0.01, update width = 1.0, dielectric constant $\varepsilon = 1$.

Modelling: The structural models of the samples **I** and **II**, which were submitted to all the simulations, were generated on the basis of the X-ray crystal structures (unit cells and atomic fractional coordinates) provided by refinement of their XRPD data by Rietveld analysis (Table 1, Table 2). All structures were 3-layered periodic supercells built up by setting $R3m$ symmetry conditions and the factors 6, 6 and 1 for the unit-cell parameters *a*, *b* and *c*, respectively. Each layer included 36 atoms of the two metals in the ratio Zn/Al = 2:1 (Figure 1) for 108 formula units. The supercell parameters $a, b, c, \alpha, \beta, \gamma$, were independent variables in the MD simulations. The interlayer water molecules and chloride (**I**) or carbonate (**II**) anions from the Rietveld analyses (Figure 2) were regularly distributed in the lattice positions denoted by green balls in Figure 1. Preliminary molecular modelling energy calculations showed that the energy-preferred position of the metallic atoms in the slab was the most regularly ordered one, i.e., that in which six Zn atoms were the nearest neighbours of each Al atom, and three Al atoms and three Zn atoms were the nearest neighbours of each Zn atom (Figure 1b). The simulated models of **I** and **II** were obtained by determining the amount of the regularly distributed interlayer water molecules for each compound by varying the sequence of the total number of water molecules (N_w) from 54, 51, 48 down to 0, and from 93, 90, 81, 72 down to 0, respectively. This corresponded to the formula coefficients (*y*) which varied from $y = 0.5$, 0.47, 0.44 down to 0 for **I**, and from $y = 0.86$, 0.83, 0.75 down to 0, for **II**. In the search for the best model, the interval over which N_w was varied was adequately restricted.

Calculation of XRPD Pattern from MD Trajectory (MD-XRPD): The cell and atomic positional parameters were calculated from the MD trajectory and stored. The angles θ and Miller indices (*h*, *k*, *l*) for which a diffraction peak should appear were determined for each of these snapshots by using the Bragg equation, $n\lambda = 2d\times\sin\theta_{(hkl)}$.

The intensity of these diffraction peaks is $I_{hkl} = |F_{hkl}|^2$, in which $F_{hkl} = \Sigma f_n e^{2\pi i(hu_n + kv_n + lw_n)}$, where *u*, *v*, *w* are atomic fractional parameters and f_n X-ray scattering factors.

The intensity obtained in this way was then stored in an array of bin size $\delta(2\theta)$ at the position corresponding to $2\theta(N) = 2\theta_{(hkl)} \pm \frac{1}{2}\delta(2\theta)$. Averaging all of the snapshots of the MD simulation completed the above MD-XPRD procedure. The diffraction intensity $I(2\theta)$, obtained in this way, was then scaled[39] for the Lorentz [$L = 1/(\sin\theta \times \sin 2\theta)$] and polarization [$p$] corrections (Lp).

Crystallite Size Broadening: The above procedure led to an MD-determined XRPD pattern for a perfect crystal of infinite dimension, whose atomic and cell parameters fluctuated due to thermal motions. When crystallites are less than approximately 1000 Å in size, appreciable broadening in the XRPD lines will occur. The shape of the peaks take on a predominantly Lorentzian profile[40] centred at $\theta_{(hkl)}$, with a full width at the half maximum (FWHM) that depends on the crystallite size. The relation that quantitatively describes the FWHM [$\Delta(2\theta_{hkl})$] as a function of the dimensions of the crystal and the order of the diffraction peak (hkl) is[40]

$$\Delta(2\theta_{hkl}) = \frac{\lambda}{\cos\theta_{hkl}} \frac{1}{d_{hkl}} \left[h^2\left(\frac{L_a}{a}\right)^2 + k^2\left(\frac{L_b}{b}\right)^2 + l^2\left(\frac{L_c}{c}\right)^2 \right]^{-\frac{1}{2}}$$

in which h, k and l are the Miller indices, and L_a, L_b, L_c are the crystallite dimensions along a, b and c, respectively. The procedure for calculating the size-broadened MD-XRPD pattern, given the dimensions L_a, L_b and L_c of the crystallite, was the same as that for a perfect crystal, whereas the values of the intensity profile of the broadened peaks were stored in the array along the bins centred around $2\theta(K) = 2\theta_{(hkl)}$ for a width of $\pm 10\,\Delta(2\theta_{hkl})$.

Modelling the XRPD Pattern: The experimental XRPD pattern (line shape and peak heights) was modelled by calculating a set of XRPD patterns from the MD trajectory that corresponded to different crystallite sizes (N patterns for N crystal sizes). Subsequently the calculated pattern was compared with the experimental XRPD curve by using the equation having the best fit for the coefficients w_i.

$$I(\theta)_{calcd} = w_1\, I_1(\theta) + w_2\, I_2(\theta) + \cdots + w_N\, I_N(\theta) = \sum_{i=1}^{N} w_i\, I_i(\theta)$$

Acknowledgments

This work was supported by the MIUR (Italy) within the PRIN Program (prot. 2004031878_002). Thanks also go to Prof. Kenny B. Lipkowitz for useful suggestions and discussions.

---

[1] H. F. W. Taylor, *Miner. Mag.* **1969**, *37*, 338–342.
[2] R. Allmann, *Chimia* **1970**, *24*, 99–342.
[3] G. Mascolo, O. Marino, *Miner. Mag.* **1980**, *43*, 619–621.
[4] W. T. Reichle, *Solid State Ionics* **1986**, *22*, 135–141.
[5] K. J. Martin, T. J. Pinnavaia, *J. Am. Chem. Soc.* **1986**, *108*, 541–542.
[6] M. Meyn, K. Beneke, G. Lagaly, *Inorg. Chem.* **1990**, *29*, 5201–5207.
[7] F. Cavani, F. Trifirò, A. Vaccari, *Catalysis Today* **1991**, *11*, 173–301.
[8] S. P. Newman, W. Jones, *New J. Chem.* **1998**, *22*, 105–115.
[9] U. Costantino, F. Marmottini, M. Nocchetti, R. Vivani, *Eur. J. Inorg. Chem.* **1998**, 1439–1446.
[10] *Layered Double Hydroxides: Present and Future* (Ed.: V. Rives), Nova Science Publishers Inc., New York, **2001**, p. 439 .
[11] A. I. Khan, D. O'Hare, *J. Mater. Chem.* **2002**, *12*, 3191–3198.
[12] V. R. L. Constantino, T. J. Pinnavaia, *Inorg. Chem.* **1995**, *34*, 883–892.
[13] W. Kagunya, Z. Hassan, W. Jones, *Inorg. Chem.* **1996**, *35*, 5970–5974.
[14] A. Vaccari, *Appl. Clay Sci.* **1999**, *14*, 161–198.
[15] B. F. Sels, D. E. De Vos, P. A. Jacobs, *Catalysis Reviews* **2001**, *43*, 443–488.
[16] D. Tichit, B. Coq, *CATTECH* **2003**, *7*, 206–217.
[17] S. Velu, K. Suzuki, M. Okazaki, M. P. Kapoor, T. Osaki, F. Ohashi, *J. Catal.* **2000**, *194*, 373–384.
[18] S. Murcia-Mascaros, R. M. Navarro, L. Gomez-Sainero, U. Costantino, M. Nocchetti, J. L. G. Fierro, *J. Catal.* **2001**, *198*, 338–347.
[19] M. Turco, G. Bagnasco, U. Costantino, F. Marmottini, T. Montanari, G. Ramis, G. Busca, *J. Catal.* **2004**, *228*, 43–55.
[20] R. Caminiti, M. Gleria, K. B. Lipkowitz, G. M. Lombardo, G. C. Pappalardo, *J. Am. Chem. Soc.* **1997**, *119*, 2196–2204.
[21] R. Caminiti, M. Gleria, K. B. Lipkowitz, G. M. Lombardo, G. C. Pappalardo, *Chem. Mater.* **1999**, *11*, 1492–1497.
[22] M. E. Amato, R. Caminiti, G. A. Carriedo, F. J. García-Alonso, J. L. García-Alvarez, G. M. Lombardo, G. C. Pappalardo, *Chem. Eur. J.* **2001**, *7*, 1486–1494.
[23] M. E. Amato, G. A. Carriedo, F. J. García-Alonso, J. L. García-Alvarez, G. M. Lombardo, G. C. Pappalardo, *J. Chem. Soc. Dalton Trans.* **2002**, 3047–3053.
[24] G. A. Carriedo, F. J. García-Alonso, J. L. García-Alvarez, G. M. Lombardo, G. C. Pappalardo, F. Punzo, *Chem. Eur. J.* **2004**, *10*, 3775–3782.
[25] G. Alberti, A. Grassi, G. M. Lombardo, G. C. Pappalardo, R. Vivani, *Inorg. Chem.* **1999**, *38*, 4249–4255.
[26] G. Alberti, G. M. Lombardo, G. C. Pappalardo, R. Vivani, *Chem. Mater.* **2002**, *14*, 295–303.
[27] S. P. Newman, H. C. Greenwell, P. V. Coveney, W. Jones, in: *Layered Double Hydroxides: Present and Future* (Ed.: V. Rives), Nova Science Publishers, Inc. New York, **2001**, Chapter 2, p. 93 and references cited therein.
[28] A. G. Kalinichev, R. J. Kirkpatrick, R. T. Cygan, *Am. Mineralogist* **2000**, *85*, 1046–1052.
[29] A. M. Fogg, A. L. Rohl, G. M. Parkinson, D. O'Hare, *Chem. Mater.* **1999**, *11*, 1194–1200.
[30] A. G. Kalinichev, J. Wang, R. J. Kirkpatrick, R. T. Cygan, in: *Foundations of Molecular Modeling and Simulations* (Ed.: P. T. Cummings), AIChE Symposium Series No. 325, **2001**, v. 97, 251 pp.
[31] A. G. Kalinichev, J. Wang, R. J. Kirkpatrick, X. Hou, *Chem. Mater.* **2001**, *13*, 145–150.
[32] J. Wang, A. G. Kalinichev, J. E. Amonette, R. J. Kirkpatrick, *Am. Mineralogist* **2003**, *88*, 398–409.
[33] R. T. Cygan, J. J. Liang, A. G. Kalinicev, *J. Phys. Chem. B* **2004**, *108*, 1255–1266.
[34] A. Larson, R. B. Von Dreele, *GSAS, Generalized Structure Analysis System*, Los Alamos National Laboratory, **1988**.
[35] R. Stahl, C. Jung, H. D. Lutz, W. Kockelmann, H. Jacobs, *Z. Anorg. Allg. Chem.* **1998**, *624*, 1130–1136.
[36] A. Noerlund Christensen, *Acta Chem. Scandinavica* **1969**, *23*, 2016–2020.
[37] W. Nowacki, J. N. Silverman, *Z. Kristallogr.* **1962**, *117*, 238–240.
[38] W. Nowacki, J. N. Silverman, *Z. Kristallogr.* **1961**, *115*, 21–51.
[39] Accelrys Inc., *MS Modeling Theory in Reflex*, San Diego: Accelrys Inc., **2003**.
[40] *The Rietveld Method* (Ed.: R. A. Young), IUCr Monograph on Crystallography, 5, Oxford University Press, **1993**.
[41] D. R. Roberts, R. G. Ford, L. Sparks, *J. Colloid. Interface Sci.* **2003**, *263*, 364–376.

Received: July 26, 2005
Published Online: November 23, 2005